RSC Applied Polymers

ROYAL SOCIETY OF CHEMISTRY

COMMUNICATION

View Article Online
View Journal | View Issue

Cite this: *RSC Appl. Polym.*, 2025, **3**, 592

Received 20th January 2025,
Accepted 26th March 2025

DOI: 10.1039/d5lp00011d

rsc.li/rscapplpolym

Harnessing mechanochemical fluorescence toward autonomous damage-reporting coatings†

Zeyu Wang, [a] Junfeng Zhou,‡[a] Zichen Ling, [b] Qixin Zhou *[b] and Junpeng Wang *[a]

Protective coatings are essential for shielding engineering materials from environmental and mechanical damage. A significant endeavor in this regard is detecting the damage in coatings and implementing necessary repairs. However, conventional detection methods often require specialized equipment and expertise, rendering them impractical for real-time monitoring. This work introduces an autonomous damage-reporting coating system based on a stress-responsive polymer network containing a Diels–Alder adduct mechanophore. When subjected to mechanical damage, the mechanophore undergoes a retro-Diels–Alder reaction, liberating a fluorescent π-extended anthracene moiety. The mechanically triggered "off-to-on" optical signal allows for highly sensitive detection of material damage preceding failure. A quantitative relationship between the extent of impact damage and the mechanochemically generated fluorescence is established, facilitating the prediction of material failure. Remarkably, the damage-reporting functionality is maintained even after incorporating pigments into the coating formulation, thereby broadening the applicability of this smart coating system in real-world scenarios.

Introduction

Reliably assessing material integrity is crucial in fields such as aerospace, automotives, and civil engineering, where structural components must withstand environmental wear, mechanical impact, and other stresses. Regular monitoring helps prevent unexpected failures and extends the lifespan of critical assets. The ability to detect and predict damage before catastrophic failure is highly valuable. Common non-destructive techniques for damage detection, including visual inspection, acoustic emission, and radiography, have proven effective.[1–8] While these methods are effective, they often require specialized equipment, and skilled personnel, and can be time-consuming and costly, making them impractical for real-time monitoring.

The quest for improved robustness of critical engineering components has led to the development of smart materials that autonomously detect damage.[9–15] Among recent advances in autonomous damage detection, the microcapsule-based system stands out for its high visibility and stability.[11–13] When the material experiences mechanical damage (*e.g.*, cutting), the microcapsules rupture, releasing the core contents, which provide *in situ* visual enhancement of damage. However, as this strategy requires irreversible material damage to trigger the detection mechanism, it can only be used to detect damage that has occurred macroscopically and thus would be already visible by itself to some extent. Consequently, this approach fails to address a crucial aspect of the maintenance of engineering materials: the prediction and/or prevention of damage.

The exploitation of mechanically active moieties (also known as mechanophores) as inherent stress sensors has been proven effective for mapping stress and quantifying bond scission in crosslinked polymers.[16–20] These mechanophores are usually covalently embedded into the polymer matrix for efficient force transduction. When subjected to sufficient force, a mechanophore is activated, forming a new product. When the product from mechanical activation shows distinct optical properties, valuable insights into material damage can be gained at the molecular level. As the onset of microscopic chain scissions precedes that of macroscopic material fracture, mechanophores have the potential to predict material damage in advance of visible failure. An example of self-reporting mechanochromic coating was demonstrated recently, using spiropyran as the stress indicator.[21] However, in that system, fiber reinforcement was required to effect mechanochromism for damage detection before material failure, while the non-reinforced counterparts fractured prior to any observable

[a]*School of Polymer Science and Polymer Engineering, The University of Akron, Akron, OH, 44325, USA. E-mail: jwang6@uakron.edu*
[b]*Department of Chemical, Biomolecular, and Corrosion Engineering, The University of Akron, Akron, OH, 44325, USA. E-mail: qzhou@uakron.edu*

†Electronic supplementary information (ESI) available. See DOI: https://doi.org/10.1039/d5lp00011d

‡Present address: Key Laboratory of Polymeric Materials & Application Technology of Hunan Province, Key Laboratory of Advanced Organic Functional Materials of College of Hunan Province, College of Chemistry, Xiangtan University, Xiangtan 411105, Hunan Province, P. R. China.

signal. The mechanophore was physically blended with the resin, which led to less efficient force transmission from the polymer matrix to the mechanophore molecules. In addition, spiropyran's lack of thermal and optical stability makes it impractical for use in coating applications.[22–25]

An ideal mechanophore for damage reporting should be thermally and optically stable, yet mechanically responsive, ensuring consistent performance during long-term storage. Upon activation under mechanical stress, the mechanophore produces a visible or spectroscopically detectable product that does not undergo reversible reactions. Anthracene–maleimide cycloadducts (AM) are stable up to 200 °C,[26] and have been shown to undergo mechanochemical retro-Diels–Alder (rDA) cycloreversion to liberate an anthracene moiety in polymer solutions,[27–31] at solid interfaces,[32,33] in micelles,[30] and in polymer networks.[20] In addition to AM, Diels–Alder adducts of anthracene with other dienophiles, such as those with triazolinedione[34,35] and acetylenedicarboxylate,[36] have also been applied as mechanochromophores. Anthracene enables the detection and quantification of bond scissions through fluorescence measurements.[20] Mechanophores based on cycloadducts of π-extended anthracene (Fig. 1), which exhibit a higher quantum yield and resistance to oxygen quenching compared to the bare anthracene, were employed to achieve more sensitive detection of molecular/material fracture.[17,37–39] Our constrained geometries simulate external force (CoGEF)[40] calculations show that the force required to activate π-extended anthracene–maleimide cycloadduct (π-AM) is lower than that for AM (3.8 nN *vs.* 4.2 nN, Fig. S1†). This increased reactivity of π-AM is expected to further enhance its sensitivity in detecting mechanical damage.

We envision that incorporating the π-AM as a highly stress-sensitive unit in a polymer coating will enable facile reporting of impact-induced material damage. When damage-induced stress is transmitted from polymer network strands to the π-AM moiety, an rDA reaction occurs, liberating a π-extended anthracene moiety (Fig. 1). This force-induced transformation converts a nonfluorescent molecule into a fluorescent one, creating an "off-to-on" optical signal for material stress detection.

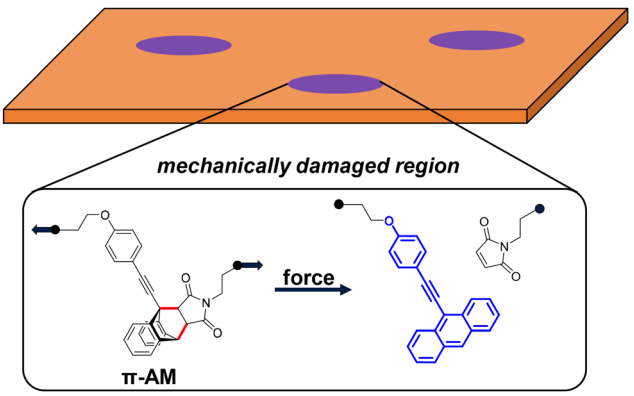

Fig. 1 Reporting mechanical damage in materials using force-induced fluorescence from a π-extended anthracene–maleimide (π-AM) mechanophore.

Results and discussion

The mechanophore π-AM utilized in this work is based on a Diels–Alder (DA) adduct of 9-π-extended anthracene that has been previously reported by Göstl *et al.*[37] A slight modification of the original structure converted the aryl alcohol to an aliphatic one, allowing the two hydroxyl groups (one on the maleimide side and the other on the anthracene side) to be equivalently reactive for crosslinking reactions (*e.g.*, condensation reaction with isocyanate). This leads to the production of a robust coating material, in which the mechanophores are uniformly distributed in the polymer network. Details on the synthesis and characterization of π-AM are provided in the ESI.†

Polyurethane (PU) has been widely used as a protective coating material, for its excellent tunability in mechanical and adhesive properties and ease of application to a wide variety of surfaces.[41–44] We, therefore, implement π-AM mechanophore in a PU matrix, as a proof of concept, to demonstrate the damage-reporting capability of a mechanophore-embedded coating. The formulation consisted of a triol crosslinker, π-AM diol, a diol chain extender, a polyol, and a diisocyanate (Fig. 2a).

We first set out to fabricate free-standing samples for initial experiments on stretching and compression (Fig. S2 and S3†). The crosslinked materials were readily obtained by curing in a Teflon mold (see ESI† for the detailed procedure). While the virgin sample exhibited an almost flat line in fluorescence spectroscopy, the specimen that was stretched to failure showed characteristic peaks of the π-extended anthracene (Fig. 2b and c). However, it is not ideal that mechanochemical fluorescence is only observed close to or beyond material fracture, as this limits the use of molecular damage detection as an indication of future material failure. Interestingly, the compressed sample exhibited a greater intensity in the mechanically generated fluorescence, which was also visible to the naked eye under UV radiation (λ_{max} = 365 nm) (Fig. 2b). This indicates that compression, one common cause of mechanical damage in coating materials, is an effective means of imparting mechanochemical activation. It is noteworthy that the intense fluorescence was generated without macroscopically rupturing the material, even under harsh compression conditions (ratio of initial to final height H_0/H = 16, held for 1 minute).

Having established the mechanochemical generation of fluorescence signal in mechanophore-linked PU without macroscopic damage, we were encouraged to investigate the damage-reporting capabilities in coatings subjected to impact. Impact represents a common and significant mode of damage that coatings endure during their service life, involving a form of transient yet destructive compression. By varying the weight and height of the falling object, we can conveniently control

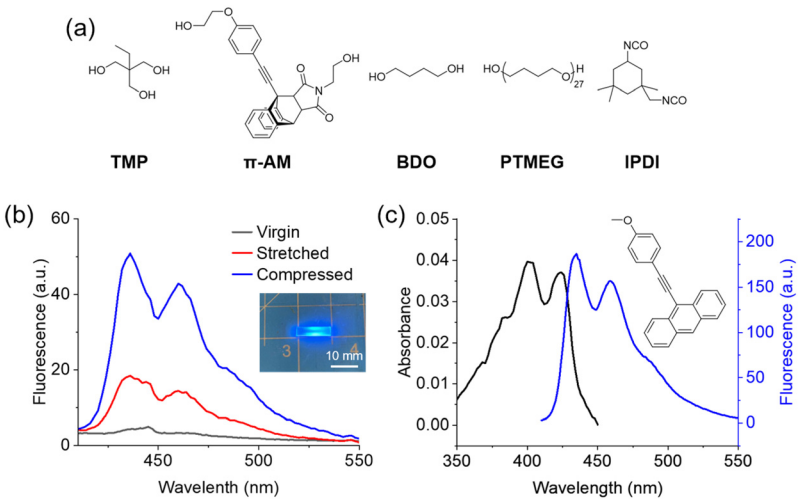

Fig. 2 Stress-responsive polyurethane material that contains π-AM mechanophore. (a) Starting materials for the mechanophore-containing polyurethane. (b) Fluorescence spectra (λ_{ex} = 400 nm) of a mechanophore-containing polyurethane material before (shown in black) and after applying stress, including stretching to fracture (shown in red) and compression to H_0/H = 16 and held for 1 minute (shown in blue). The inset photo shows the compressed piece irradiated by a UVA flashlight (λ_{max} = 365 nm). (c) Absorbance and fluorescence spectra of the reference compound in THF solution, indicating the successful mechanochemical generation of fluorescent π-extended anthracene.

the extent of damage, which could be quantified by the mechanically triggered fluorescence signal. We hypothesize that the correlation between mechanical damage and the optical signal provides a promising method for reporting and potentially predicting damage in a protective coating system.

The PU coating, incorporating covalently linked π-AM, was applied onto a steel substrate and cured at 120 °C for 30 minutes. Impact damage was introduced using an impact tester (Fig. S4†). It was anticipated that molecular-level damage would be visualized through mechanochemical fluorescence, even in the absence of observable macroscopic damage visible to the naked eye. Various weights, including 0.5 kg, 1.0 kg, and 2.0 kg, were used to free-fall onto a punch placed on the PU coating from heights ranging from 25 to 100 mm. While the strike led to indentations on the underlying steel plate, the coating itself remained largely intact (Fig. 3a). When irradiated with UV light (λ_{max} = 365 nm), the impacted region exhibited a blue fluorescence, indicating that π-AM in the PU coating was activated by the impact. The circular fluorescence pattern is likely a result of non-uniform deformation caused by the round-nosed punch. Mechanochemical activation was concentrated at the periphery, indicating that the shear stress was highest at the edge of the punched area.

Our ultimate goal is to establish a quantitative correlation between the impact energy and the material damage. The impact energy (IE) can be expressed as IE = $m{\cdot}g{\cdot}h$, assuming all gravitational potential energy is converted into energy to cause material deformation. Thus, the impact energy can be modulated by varying the mass of the falling object (m) and the drop height (h). Qualitatively, we observed that as either the weight of the falling object or the drop height increased, the fluorescence intensity in the impacted area also increased (Fig. S5†). At m = 0.5 kg and h = 25 mm, the blue fluorescence was barely observable, whereas at m = 2.0 kg and h = 100 mm, it became significantly brighter (Fig. 3b).

Fluorescence microscopy and RGB analysis were performed to quantify the extent of damage that was manifested by the mechanically generated fluorescence. As shown in Fig. 3c, the relationship between fluorescence intensity and impact energy, for various combinations of m and h, was well-described by linear regression. We believe this method can be generalized to other systems, as the linear relationship between fluorescence intensity and impact energy offers a promising approach for predicting material failure. It is noteworthy that a relatively low loading of the mechanophore (1 wt%) was sufficient for sensitive detection of damage, ensuring that the properties of the parent material remain largely unchanged and uncompromised by the addition of the mechanically responsive moiety.

Coatings used in real-world applications are often colored for aesthetics and/or for functionalities like anti-aging or UV protection. Unlike many previously reported smart coating systems, the mechanophore-incorporated PU in this work is colorless and transparent (Fig. S6†). It can therefore be easily colored by commercial pigments to broaden the potential uses of the damage-reporting system. For demonstration, white, blue, and orange pigments were selected to cover a broad range of the visible spectrum (Fig. S8†). Detailed information about the pigments used is enclosed in the ESI.†

A primary concern was that the absorbance of the pigments might interfere with the excitation and emission of the π-extended anthracene, which is responsible for the damage-reporting performance of the coating. However, despite the strong absorbance of the pigmented coatings in the wavelength range relevant to the fluorescence of the π-extended anthracene (Fig. S6†), the pigments did not hinder damage

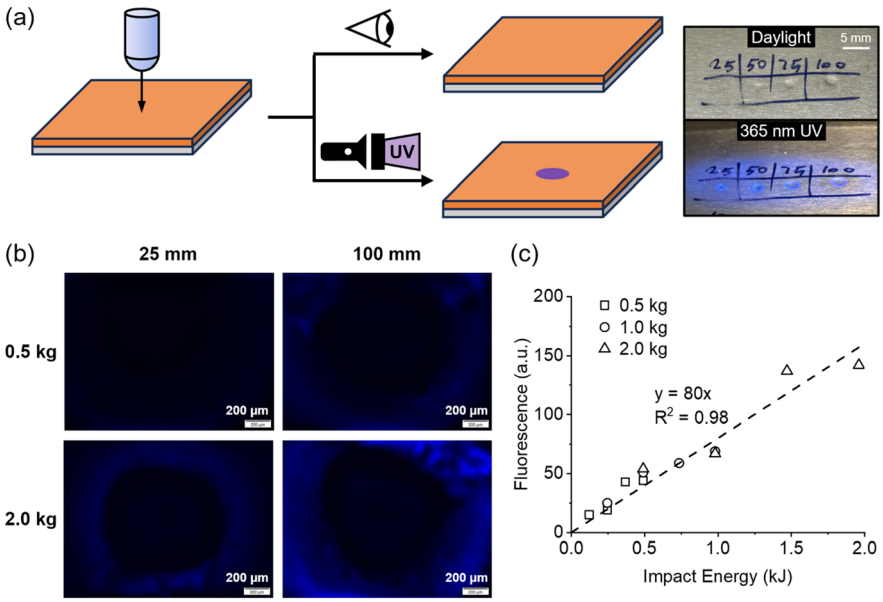

Fig. 3 Detection of impact damage by mechanochemical fluorescence. (a) The impact experiments to quantify the effect of impact on mechanochemical fluorescence response in mechanophore-containing coatings. (b) Fluorescence microscopic images of the impact areas of the clear coating that was struck by a falling punch of two different weights and from two different heights. Scale bar = 200 μm. (c) The profile of change in fluorescence intensity as a function of the impact energy.

visualization (Fig. 4a). The fluorescence spots were clearly visible in all pigmented coatings subjected to impact damage.

Images captured by an iPhone (Fig. 4a), representing what the naked eye observes, differed from those taken using a fluorescence microscope (Fig. 4b). While the fluorescence in the white coating was visible in both types of imaging, the blue and orange coatings did not show significant fluorescence under the fluorescence microscope. The likely explanation is that the high absorbance in the UV-to-blue region by these two pigments (Fig. S6†) interfered with fluorescence detection using the fluorescence microscope, which uses a filter set (λ_{ex}: 360–370 nm, λ_{em}: 420–460 nm) (Fig. S7†). Without the filter, the absorbance of the emitted blue fluorescence by the pigments creates a color contrast, making the damaged regions visible. The limited effectiveness of fluorescence microscopy in this case is not a major concern, as the damage-induced fluorescence remains clearly visible to the naked eye.

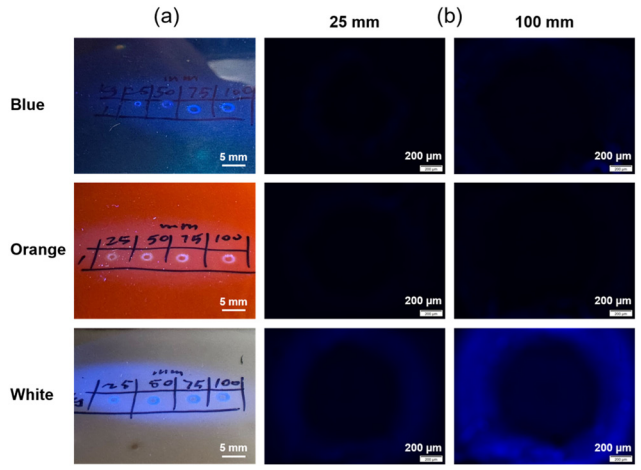

Fig. 4 Damage detection of pigmented coatings. (a) iPhone photos of the coatings with blue, orange, and white pigments after impact by a punch of 1.0 kg falling from varying heights, as indicated by the numbers above the spots of impact. Mechanically generated fluorescence was visualized under UV light (λ = 365 nm) at the points of impact. (b) Fluorescence microscopy images of the impact areas of pigmented coatings that were struck by a 1.0 kg punch from two different drop heights as indicated above the corresponding images.

Conclusions

In this work, we demonstrated an autonomous damage-reporting system based on a mechanochemically responsive polymer network incorporating a π-extended mechanophore. This system enables the generation of a fluorescent signal upon mechanical impact, without requiring visible material fracture. The mechanochemically generated fluorescence showed a linear correlation with impact energy, offering potential for precise damage prediction based on optical signals. Importantly, the damage-reporting functionality remained effective even with the addition of commercial pigments, ensuring broad applicability in real-world scenarios. This mechanochemical approach provides a straightforward and efficient method for autonomous damage detection and prediction, eliminating the need for specialized equipment or skilled personnel. The low loading of mechanophore required for sensitive detection suggests minimal impact on the material's intrinsic properties. By using a mechanophore as a

reactive additive, this strategy is adaptable to a wide range of polymeric formulations. Additionally, it aligns with sustainability goals by enabling lightweight, energy-efficient designs, minimizing excess material usage, and reducing costly, time-intensive inspections. Damage detection can be achieved easily with a handheld UV light. Moving forward, we expect that this approach can be applied to any scenario where surface integrity is essential, such as in rotor blades, vehicle panels, and safety equipment. Since only the outermost layers need mechanophore functionality to serve as a damage sensor, the bulk of the material remains unmodified.

Author contributions

Z. W., Q. Z. and J. W. conceived the project. Z. W. and J. Z. prepared the polyurethane materials. Z. W. synthesized the mechanophore. Z. W. and Z. L. conducted the impact experiments. Z. W. performed the characterization and analysis. Z. W. and J. W. wrote the manuscript. Z. W. wrote the original draft. All authors reviewed and edited the manuscript.

Data availability

The data supporting this article have been included as part of the ESI.†

Conflicts of interest

There are no conflicts to declare.

Acknowledgements

This work was supported by the National Science Foundation under Grant No. CHE-2204079. J. W. acknowledges the Alfred P. Sloan Foundation for a Sloan Research Fellowship (FG-2023-20341) and the Camille and Henry Dreyfus Foundation for a Camille Dreyfus Teacher-Scholar Award (TC-24-087).

References

1 R. Brown, *Handbook of polymer testing: physical methods*, CRC press, 1999.
2 R. Yang, Y. He and H. Zhang, *Renewable Sustainable Energy Rev.*, 2016, **60**, 1225–1250.
3 P. Duchene, S. Chaki, A. Ayadi and P. Krawczak, *J. Mater. Sci.*, 2018, **53**, 7915–7938.
4 S. K. Dwivedi, M. Vishwakarma and P. A. Soni, *Mater. Today: Proc.*, 2018, **5**, 3690–3698.
5 G. Goch, B. Schmitz, B. Karpuschewski, J. Geerkens, M. Reigl, P. Sprongl and R. Ritter, *Precis. Eng.*, 1999, **23**, 9–33.
6 S. S. Jamali, Y. Zhao, Z. Gao, H. Li and A. C. Hee, *J. Ind. Eng. Chem.*, 2016, **43**, 36–43.
7 M. I. Silva, E. Malitckii, T. G. Santos and P. Vilaça, *Prog. Mater. Sci.*, 2023, **138**, 101155.
8 J. Zhu, Z. Mao, D. Wu, J. Zhou, D. Jiao, W. Shi, W. Zhu, Z. Liu, J. Zhu, Z. Mao, D. Wu, J. Zhou, D. Jiao, W. Shi, W. Zhu and Z. Liu, *J. Nondestr. Eval.*, 2022, **41**, 49.
9 O. Rifaie-Graham, E. A. Apebende, L. K. Bast and N. Bruns, *Adv. Mater.*, 2018, **30**, 1705483–1705483.
10 L. Ma, C. Ren, J. Wang, T. Liu, H. Yang, Y. Wang, Y. Huang and D. Zhang, *Chem. Eng. J.*, 2021, **421**, 127854–127854.
11 W. Li, C. C. Matthews, K. Yang, M. T. Odarczenko, S. R. White and N. R. Sottos, *Adv. Mater.*, 2016, **28**, 2189–2194.
12 M. J. Robb, W. Li, R. C. R. Gergely, C. C. Matthews, S. R. White, N. R. Sottos and J. S. Moore, *ACS Cent. Sci.*, 2016, **2**, 598–603.
13 X. Lu, W. Li, N. R. Sottos and J. S. Moore, *ACS Appl. Mater. Interfaces*, 2018, **10**, 40361–40365.
14 O. J. Dodo, I. O. Raji, I. J. Arny, C. P. Myers, L. Petit, K. Walpita, D. Dunn, C. J. Thrasher and D. Konkolewicz, *RSC Appl. Polym.*, 2023, **1**, 30–45.
15 D. Li, Z. Zhang, B. Sukhbat, X. Wang, X. Zhang, J. Yan, J. Zhang, Q. Zhang, Y. Li, H. Wang and Y. Yan, *RSC Appl. Polym.*, 2025, Advance Article, DOI: **10.1039/D4LP00351A**.
16 E. Ducrot, Y. Chen, M. Bulters, R. P. Sijbesma and C. Creton, *Science*, 2014, **344**, 186–189.
17 J. Slootman, V. Waltz, C. J. Yeh, C. Baumann, R. Göstl, J. Comtet and C. Creton, *Phys. Rev. X*, 2020, **10**, 41045–41045.
18 Y. Chen, C. Joshua Yeh, Y. Qi, R. Long and C. Creton, *Sci. Adv.*, 2020, **6**, 1–9.
19 J. Slootman, C. J. Yeh, P. Millereau, J. Comtet and C. Creton, *Proc. Natl. Acad. Sci. U. S. A.*, 2022, **119**, 1–11.
20 C. P. Kabb, C. S. O'Bryan, C. D. Morley, T. E. Angelini and B. S. Sumerlin, *Chem. Sci.*, 2019, **10**, 7702–7708.
21 S. Shree, M. Dowds, A. Kuntze, Y. K. Mishra, A. Staubitz and R. Adelung, *Mater. Horiz.*, 2020, **7**, 598–604.
22 N. Tamaoki, E. Van Keuren, H. Matsuda, K. Hasegawa and T. Yamaoka, *Appl. Phys. Lett.*, 1996, **69**, 1188–1190.
23 S. Yagi, K. Maeda and H. Nakazumi, *J. Mater. Chem.*, 1999, **9**, 2991–2997.
24 L. Kortekaas, W. R. Browne, L. Kortekaas and W. R. Browne, *Chem. Soc. Rev.*, 2019, **48**, 3406–3424.
25 K. Kinashi, Y. Harada and Y. Ueda, *Thin Solid Films*, 2008, **516**, 2532–2536.
26 J. A. Syrett, G. Mantovani, W. R. Barton, D. Price and D. M. Haddleton, *Polym. Chem.*, 2010, **1**, 102–106.
27 A. C. Overholts, M. E. McFadden and M. J. Robb, *Macromolecules*, 2022, **55**, 276–283.
28 J. Li, T. Shiraki, B. Hu, R. A. E. Wright, B. Zhao and J. S. Moore, *J. Am. Chem. Soc.*, 2014, **136**, 15925–15928.
29 D. C. Church, G. I. Peterson and A. J. Boydston, *ACS Macro Lett.*, 2014, **3**, 648–651.
30 H. Li, R. Göstl, M. Delgove, J. Sweeck, Q. Zhang, R. P. Sijbesma and J. P. A. Heuts, *ACS Macro Lett.*, 2016, **5**, 995–998.

31 D. Xu, W. Liu, S. Tian and H. Qian, *Angew. Chem.*, 2025, **64**, e202415353.
32 J. Sung, M. J. Robb, S. R. White, J. S. Moore and N. R. Sottos, *J. Am. Chem. Soc.*, 2018, **140**, 5000–5003.
33 A. R. Sulkanen, J. Sung, M. J. Robb, J. S. Moore, N. R. Sottos and G. Y. Liu, *J. Am. Chem. Soc.*, 2019, **141**, 4080–4085.
34 G. R. Gossweiler, G. B. Hewage, G. Soriano, Q. M. Wang, G. W. Welshofer, X. H. Zhao and S. L. Craig, *ACS Macro Lett.*, 2014, **3**, 216–219.
35 S. Chakraborty, S. Choudhury and N. K. Singha, *Small*, 2024, **20**, 2406866.
36 F. Yang, T. Geng, H. Shen, Y. Kou, G. Xiao, B. Zou and Y. Chen, *Angew. Chem., Int. Ed.*, 2023, **62**, e202308662.
37 R. Göstl and R. P. Sijbesma, *Chem. Sci.*, 2016, **7**, 370–375.
38 M. Stratigaki, C. Baumann, L. C. A. Van Breemen, J. P. A. Heuts, R. P. Sijbesma and R. Göstl, *Polym. Chem.*, 2020, **11**, 358–366.
39 A. Cartier, O. Taisne, S. Ivanov, J. Caillard, M. Couty, J. Comtet and C. Creton, *Macromolecules*, 2024, **57**, 8712–8721.
40 I. M. Klein, C. C. Husic, D. P. Kovács, N. J. Choquette and M. J. Robb, *J. Am. Chem. Soc.*, 2020, **142**, 16364–16381.
41 A. Das and P. Mahanwar, *Adv. Ind. Eng. Polym. Res.*, 2020, **3**, 93–101.
42 E. A. Papaj, D. J. Mills and S. S. Jamali, *Prog. Org. Coat.*, 2014, **77**, 2086–2090.
43 S. Zafar, R. Kahraman and R. A. Shakoor, *Eur. Polym. J.*, 2024, **220**, 113421.
44 D. K. Chattopadhyay and K. V. S. N. Raju, *Prog. Polym. Sci.*, 2007, **32**, 352–418.